Mon. Not. R. Astron. Soc. **357,** 1038–1048 (2005) doi:10.1111/j.1365-2966.2005.08735.x

Transforming observational data and theoretical isochrones into the ACS/WFC Vega-mag system

Luigi R. Bedin,[1⋆†] Santi Cassisi,[2†] Fiorella Castelli,[3,4†] Giampaolo Piotto,[1] Jay Anderson,[5†] Maurizio Salaris,[6†] Yazan Momany[1] and Adriano Pietrinferni[2]

[1]*Dipartimento di Astronomia, Università di Padova, vicolo dell'Osservatorio 2, I-35122 Padova, Italy*
[2]*INAF-Osservatorio Astronomico di Collurania, via M. Maggini, 64100 Teramo, Italy*
[3]*Istituto di Astrofisica Spaziale e Fisica Cosmica, CNR, via del Fosso del Cavaliere, I-00133 Roma, Italy*
[4]*INAF-Osservatorio Astronomico di Trieste, via Tiepolo 11, 34131 Trieste, Italy*
[5]*Department of Physics and Astronomy, Mail Stop 108, Rice University, 6100 Main Street, Houston, TX, 77005, USA*
[6]*Astrophysics Research Institute, Liverpool John Moores University, 12 Quays House, Birkenhead CH41 1LD*

Accepted 2004 December 7. Received 2004 October 26; in original form 2004 May 24

ABSTRACT

We propose a zero-point photometric calibration of the data from the Advanced Camera for Surveys (ACS) Wide Field Channel (WFC) on board the *Hubble Space Telescope*, based on a spectrum of Vega and the most up-to-date in-flight transmission curves of the camera. This calibration is accurate at the level of a few hundredths of a magnitude. The main purpose of this effort is to transform the entire set of evolutionary models into a simple observational photometric system for ACS/WFC data, and to make them available to the astronomical community. We provide the zero-points for the most used ACS/WFC bands, and give basic recipes for calibrating both the observed data and the models. We also present the colour–magnitude diagram from ACS data of five Galactic globular clusters, spanning the metallicity range $-2.2 <$[Fe/H] < -0.04, and we provide fiducial points representing their sequences from several magnitudes below the turn-off to the red giant branch tip. The observed sequences are compared with the models in the newly defined photometric system.

Key words: techniques: photometric – Hertzsprung–Russell (HR) diagram – stars: imaging.

1 INTRODUCTION

After two and a half years of operation, the Advanced Camera for Surveys (ACS) on board the *Hubble Space Telescope* (*HST*) has collected a huge number of observations of stellar systems, and produced a growing data base of colour–magnitude diagrams (CMDs) and luminosity functions. In order to be able to exploit fully the information contained in these data sets, and to extract a number of fundamental parameters we are interested in, such as metal content, ages, distances, mass functions, etc., we need to compare the observations with theoretical models. The basic requirement for this comparison is the conversion of stellar models into the ACS photometric observational domain. This conversion is the purpose of the present paper. We have used the most up-to-date information on the ACS specifications to define a natural, in-flight photometric system and to transform the Pietrinferni et al. (2004) models into the same system. While it is foreseeable that the ACS photometric calibration will improve as more standard fields are studied and cross-compared, the in-flight transmission efficiency curves are now reasonably well established and we would not expect them to change very much. It therefore makes sense to provide a conversion of theoretical stellar models into the observational domain so that more quantitative and qualitative interpretations can be made of observations.

It is worth mentioning that most astronomical photometric investigations are based on some 'standard' photometric system. Here, by standard, we mean a photometric system that has been widely used for a long time in different observatories (e.g. the Johnson–Kron–Cousins, Strömgren, Thuan–Gunn, etc., systems; see, for example, Landolt 1992), and possibly defined by a number of standard stars well distributed in the sky, whose flux has been carefully measured. The calibration to a standard system is sometimes the only way to interpret properly the collected data, e.g. when we need to compare our photometric sequences with others collected with different instruments or at different epochs, or with standard results from theoretical models. Still, it must be clearly stated that when the transmission curves of the equipment used to collect the observations are rather different from those of any existing standard system, the transformation of the data to a standard system is difficult, and can be unreliable, particularly for extreme stars (i.e. extreme colours, unusual spectral type, high reddening, etc.).

⋆E-mail: lbedin@eso.org (LRB); cassisi@te.astro.it (SC); castelli@ts.astro.it (FC); piotto@pd.astro.it (GP); jay@eeyore.rice.edu (JA); ms@astro.livjm.ac.uk (MS); momany@pd.astro.it (YM); pietrinferni@te.astro.it (AP)
†Present address: European Southern Observatory, Karl-Schwarzschild-Strasse 2, 85748 Garching b. München, Germany.

A good example of a problem that one can encounter in using even slightly different filter sets at the same telescope is given in Momany et al. (2003).

Many of the ACS filters differ substantially from the 'standard' filters, and the high photometric precision possible with ACS makes the systematic differences more significant. Thankfully, the filter and instrumental response are better characterized for ACS than they are for the typical ground-based observatory, so that it is possible to avoid standard systems altogether and compare the data and the model in the same system: the observational domain. All that is required for this is to determine an empirical zero-point for each filter by observing a reference star with a well-characterized spectrum in order to characterize accurately the throughput and response of the detector for each filter. The theoretical models can then be integrated over the same spectral response and compared directly with the data. Such a procedure for comparing models with data is far preferable to the typical procedure of converting both models and data into a 'standard' system.

Therefore, we calculated a set of empirical zero-points that will allow direct comparison of observational data and theoretical models. We have based our calibration on the reference spectrum of Vega, and so we will refer to our photometric system as the 'ACS Vega-mag system'. In our derivation of zero-points, we used the in-flight sensitivity, measured by Sirianni et al. (2002) and Sirianni (private communication).

In this paper we have focused our attention on the Wide Field Channel (WFC) of the ACS, but the same procedure can be used to measure the photometric zero-points for the High-Resolution Channel (HRC).

In the next section, we describe briefly the total transmission curves and the procedure followed to obtain the zero-points, and we give the aperture corrections. In Section 3, we briefly describe the adopted stellar evolution models, our procedure to transform the models into the observational plane, and the method used to take into account interstellar absorption. In Section 4, we give the zero-points and the formulae to convert both the theoretical tracks and the observed data to the ACS Vega-mag photometric system. In Section 5 we describe the *HST* archive data used to test the models and we show, as an example, how these data have been photometrically calibrated and compared with our models in the ACS Vega-mag plane. Conclusions follow in Section 6, together with instructions on how to download the transformed models.

2 DEFINING THE ACS VEGA-MAG PHOTOMETRIC SYSTEM

In this section, we define our photometric system and we refer to it as the ACS(/WFC) Vega-mag system.

2.1 Total transmission of the *HST*+WFC/ACS

The first step toward the definition of our photometric system is to calculate the total transmission curves, $T(\lambda)$ for each individual band. These are the products of the individual transmission curves, $t_i(\lambda)$, for five different terms:

$$T(\lambda) = t_1(\lambda) \times \cdots \times t_5(\lambda).$$

In detail, the $t_i(\lambda)$ are: t_1, the transmission curve of the window of the dewar; t_2, the transmission curve of the filters; t_3, the reflectivity of the WFC/ACS mirrors (three mirrors); t_4, an average of the two CCD quantum efficiencies;[1] t_5, the transmission curve of the Optical Telescope Assembly (OTA) of the *HST*.[2] In order to outline our procedure, we consider two commonly used filters, F606W and F814W. We will extend the results to other filters in Section 4. All the individual transmission curves are shown in Fig. 1, where two thick lines show the total system transmissions for the two considered filters.

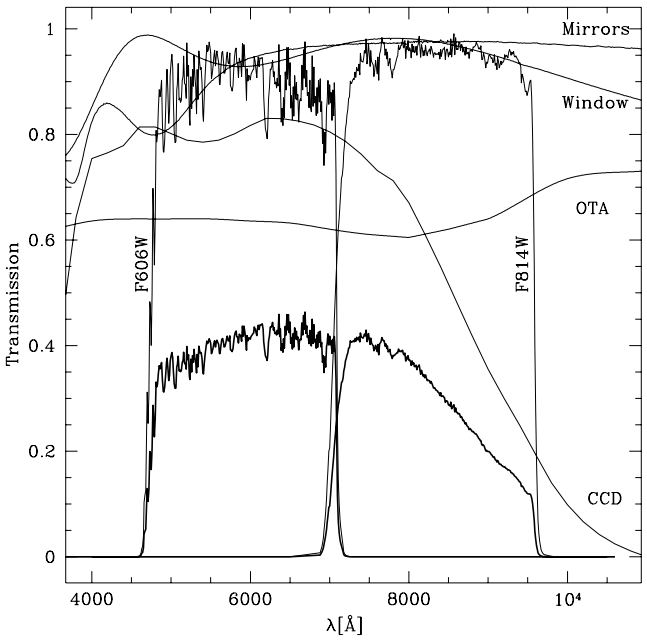

Figure 1. ACS/WFC transmission curves for the window of the dewar, of the WFC/ACS's mirrors, of the CCD, of the OTA, and finally the transmission curves for the two ACS/WFC filters, F606W and F814W. The resulting total transmission curve for the two filters is shown as a thick line.

The transmission curves measured in the laboratory differ significantly from those found on-orbit (Sirianni et al. 2002). In the following we use only the on-orbit adjusted total transmission curves obtained by Sirianni et al. (in preparation). The uncertainties for these total transmission curves are within 0.5 per cent (De Marchi et al. 2004;[3] Sirianni et al., in preparation).

2.2 Determination of zero-points

We describe below the procedure used to define the zero-points of the system.

We have used the spectrum of Vega from ftp://ftp.stsci.edu/cdbs/cdbs2/grid/k93models/standards/ vega_reference.fits. Details of this spectrum can be found at http://www.stsci.edu/instruments/observatory/PDF/ scs8.rev.pdf; hereafter, it will be denoted as $F^0(\lambda)$, in units of erg s^{-1} cm^{-2} Å^{-1}.

The integrated flux of the assumed spectrum of Vega under the total transmission curve T of the filter F606W +

[1] These curves are available at the Space Telesscope Science Institute (STScI) website, http://www.stsci.edu/hst/acs/analysis/reference_files/synphot_tables.html.

[2] This last component has been obtained from the website ftp://ftp.stsci.edu/cdbs/cdbs2/comp/ota/ tabulated in the file hst_ota_007_syn.fits.

[3] Published after the submission of the present work.

instrument is

$$I^0(\mathrm{F606W}) = \int_{-\infty}^{\infty} \cdots \simeq \int_{\lambda_{\min}}^{\lambda_{\max}} F^0(\lambda) T_{\mathrm{F606W}}(\lambda)\, \mathrm{d}\lambda$$
$$= 2.7591 \times 10^{-6}\ \mathrm{erg\ s^{-1}\ cm^{-2}}.$$

This number is the quantity that theoreticians will need to rescale their models to the photometric system we adopt (see Section 4).

The estimated number of expected photoelectrons (e^-) is

$$N^0_{e^-}(\mathrm{F606W}) = \int_{-\infty}^{\infty} \cdots \simeq \int_{\lambda_{\min}}^{\lambda_{\max}} \frac{F^0(\lambda)}{e_\gamma(\lambda)} T_{\mathrm{F606W}}(\lambda)\, \mathrm{d}\lambda$$
$$= 795\,861\ \mathrm{e^-\ s^{-1}\ cm^{-2}},$$

where the photon energy $e_\gamma\ (\lambda)$ is given by

$$e_\gamma(\lambda) = hc/\lambda \quad \mathrm{erg}.$$

Therefore, for Vega, the counts detected by the system in digital numbers (DNs) would be

$$I^0_{\mathrm{DN}}(\mathrm{F606W}) = N^0_{e^-}(\mathrm{F606W}) \times A_{\mathrm{eff}}/\mathrm{GAIN}$$
$$= 3.6004 \times 10^{10}/\mathrm{GAIN} \qquad \mathrm{DN\ s^{-1}},$$

where A_{eff} is the effective collecting area of the telescope (45 239 cm^2, with the secondary obscuration already accounted for), and GAIN is the conversion factor from e^- to DNs.

At this point, we can define the zero-point of our magnitude system in the F606W band by imposing $m_{\mathrm{F606W}} \equiv 0$ for the magnitude of Vega (with the assumed spectrum):

$$Zp^{\mathrm{F606W}} \equiv 2.5\ \log_{10} \frac{I^0_{\mathrm{DN}}(\mathrm{F606W})}{[\mathrm{DN\ s^{-1}}]} = 26.391.$$

For simplicity, we have defined this zero-point for GAIN = 1 e^-/DN.

Because FLT images provided by STScI are already in photoelectrons (e^-) rather than in DNs (note that DRZ images are given in e^- s^{-1}) hereafter, to avoid any confusion, we will not consider the GAIN, and we will refer to I^-_{e} rather than to I_{DN}.

In an analogous way we can define the zero-point of the F814W band

$$Zp^{\mathrm{F814W}} = 25.492,$$

and in a similar way for all the other filters.

2.3 Calibration of the observations

The formula that observers should use to calibrate their observations into our WFC/ACS Vega-mag system magnitudes in the F606W band is

$$m_{\mathrm{F606W}} \equiv -2.5 \log_{10} \frac{I_{e^-}}{\mathrm{exptime}} + Zp^{\mathrm{F606W}} - Z_{\mathrm{Aperture}}$$

where exptime is the exposure time and Z_{Aperture} is the aperture correction. In the next section we discuss in detail the aperture correction, which we will always treat as a positive quantity to be subtracted. This calibration is intended for the officially calibrated DRZ images which are already corrected for flat-field, dark, bias and geometrical distortion.[4]

[4] The images are still affected, at least by charge-transfer efficiency (CTE) and charge diffusion (see Krist 2003; Riess & Mack 2004). In Section 5.1 we use FLT images, and describe how we linked our photometry for those images to the officially corrected DRZ images.

Table 1. $\Delta m_{\mathrm{AP}(r)-\mathrm{AP}(\infty)}$ corrections to be added to the zero-points.

Filter	$\Delta m_{\mathrm{AP}(\infty)-\mathrm{AP}(\infty)}$	$\Delta m_{\mathrm{AP}(0.5\,\mathrm{arcsec})-\mathrm{AP}(\infty)}$	$\Delta m_{\mathrm{AP}(0.3\,\mathrm{arcsec})-\mathrm{AP}(\infty)}$
F435W	0.000	0.095	0.132
F475W	0.000	0.084	0.120
F502N	0.000	0.078	0.114
F550M	0.000	0.076	0.110
F555W	0.000	0.076	0.110
F606W	0.000	0.079	0.115
F625W	0.000	0.080	0.118
F658N	0.000	0.079	0.123
F660N	0.000	0.079	0.123
F775W	0.000	0.078	0.123
F814W	0.000	0.079	0.130

2.4 Aperture corrections

Breathing of the telescope tube, the complex optical system and charge diffusion induce temporal and spatial variations of the core of the point spread function (PSF), such that the first-ring ratio of the diffraction figure changes considerably across the chip and at a minor level with orbital phase.

For these reasons, we choose to refer our zero-points to an infinite aperture. This makes it easier for those studying surface photometry of extended sources to calibrate their magnitudes to this system. The aperture corrections for extended sources are null, being the zero-points of the system referred to an infinite aperture:[5]

$$Z_{\mathrm{Aperture}} = 0.$$

On the other hand, in practice all the energy of a point source is contained within 4 arcsec (∼80 pixel), and ∼93 per cent within 0.5 arcsec (∼10 pixel). In dense environments, where crowding makes an aperture correction to an infinite aperture impossible, one has to rely on the in-flight encircled energy.[6] This means that one has to correct the instrumental magnitude (for example, the PSF-fitted magnitude) to the magnitude at a specified aperture r by adding $\Delta m_{\mathrm{PSF}-\mathrm{AP}(r)}$, and then sum an additional quantity $\Delta m_{\mathrm{AP(r)}-\mathrm{AP}(\infty)}$, obtained from the tabulated encircled energy, in order to link the magnitudes to the infinite aperture for which we have calculated the zero-points.

In summary,

$$Z_{\mathrm{Aperture}} = \Delta m_{\mathrm{PSF}-\mathrm{AP}(r)} + \Delta m_{\mathrm{AP}(r)-\mathrm{AP}(\infty)}.$$

In Table 1 we give the $\Delta m_{\mathrm{AP}(r)-\mathrm{AP}(\infty)}$ corrections to be added to the zero-points for two circular apertures of radius 0.3 arcsec (∼6 pixel) and 0.5 arcsec (as in Holtzman et al. 1995) and for the different filters. For clarity, we also report in Table 1 the correction to zero-points for an infinite aperture, which is zero by definition.

For point sources, the $\Delta m_{\mathrm{PSF}-\mathrm{AP}(r)}$ correction should be estimated in each individual image, remembering that the smaller the aperture (r), the more the photometry is affected by the problems mentioned at the beginning of this section (i.e. spatial variability of the PSF and charge diffusion). See Section 5.2 for uncertainties on the values of $\Delta m_{\mathrm{PSF}-\mathrm{AP}(r)}$.

[5] Note that this is really only true for infinite extended sources, or sources larger than the widest part of the PSF halo.

[6] This is tabulated at the STScI website http://www.stsci.edu/hst/acs/analysis/reference_files/wfc_synphottable_list.html.

Moreover, there appears to be a second-order effect which depends on the colour of the stars and on the filter used (Sirianni, in preparation). In practice, the present calibration is useful only if the degree of accuracy desired by the observers is no better than tow to three hundredths of a magnitude. However, taking into account all the problems of the ACS, it seems hard to achieve a much higher accuracy. It should be noted that the photometric stability of the Wide Field Planetary Camera 2 (WFPC2) was certainly not any better than this, but the higher precision of WFC/ACS makes systematic errors (on the zero-points) the dominant source of error in the final photometry.

We have decided not to deal with the two filters, F850LP and F892N, because they are much more problematic (see Sirianni, in preparation).

3 TRANSFORMING THE STELLAR MODELS INTO THE ACS VEGA-MAG SYSTEM

3.1 Stellar evolution models

In this paper, we adopt the stellar-evolution model data base in Pietrinferni et al. (2004); for a detailed description of the models, as well as a comparison with other stellar model libraries available in the literature, we refer the interested reader to this reference. For the purposes of this paper, we briefly list the main characteristics of this model library.

Evolutionary tracks are available for up to 41 mass values at each of 10 selected initial chemical compositions. The minimum mass considered is roughly 0.5 $M_{\odot}$, while the maximum value is always equal to 10 $M_{\odot}$. The whole set of evolutionary computations has been used to compute isochrones for a large age range, from $\sim$40 Myr to $\sim$14 Gyr, covering all stellar evolution phases from the zero-age main sequence up to the first thermal pulse on the asymptotic giant branch or to C ignition. For each chemical composition, a zero-age horizontal branch (ZAHB) locus, as well as post-ZAHB evolutionary tracks, was also calculated for a large range of masses, by employing the He-core mass and chemical profiles in the H-rich envelope of the red giant branch (RGB) progenitor, having an age at the He flash of the order of $\sim$12–13 Gyr.

The set of models has been computed for metallicities in the range $0.0001 \leqslant Z \leqslant 0.04$ for both a scaled-solar mixture and an α-enhanced mixture ($\langle [\alpha/\mathrm{Fe}] \rangle = 0.4$; in preparation).

The adopted reference scaled-solar heavy element mixture is from Grevesse & Noels (1993). As for the He abundance, the models employ a primordial mass fraction of $Y_0 = 0.245$, based on the estimates by Cassisi, Salaris & Irwin (2003) – see also Salaris et al. (2004) – obtained from the *R*-parameter method applied to a large sample of Galactic globular clusters (GGCs). This Y_0 value is in fair agreement with recent independent determinations of the cosmological baryon density from the *Wilkinson Microwave Anisotropy Probe* (*WMAP*) results (Spergel et al. 2003). To reproduce the initial solar He abundance obtained from an appropriately calibrated solar model, an He enrichment ratio $\mathrm{d}Y/\mathrm{d}Z = 1.4$ has been used (Pietrinferni et al. 2004).

All models have been computed with outer boundary conditions obtained by integrating the atmospheric layers with the Krishna-Swamy (1966) $T(\tau)$ relationship. Superadiabatic convection is treated according to the Cox & Giuli (1968) formalism of mixing-length theory (Böhm-Vitense 1958), and the mixing-length parameter has been fixed by the solar calibration ($ml = 1.713$) and kept constant for all masses during all evolutionary phases; mass loss is included by employing the Reimers (1975) formula with the free parameter η set to 0.4.

At each chemical composition, models have been computed with and without overshooting from the convective cores during the main-sequence (MS) phase. In the former case, $\lambda_{\mathrm{OV}} = 0.20 \times H_{\mathrm{P}}$ for masses larger than 1.7 $M_{\odot}$, where λ_{OV} is the extension of the overshooting region in units of the local pressure scaleheight. For stars less massive than 1.1 $M_{\odot}$, $\lambda_{\mathrm{OV}} = 0$, while in the intermediate range λ_{OV} varies according to the relation $\lambda_{\mathrm{OV}} = (M/M_{\odot} - 0.9)/4$. This choice allows a smooth variation of the isochrone turn-off (TO) morphology, and a smooth decrease to zero of the convective core mass. This parametrization also provides a good match to the TO morphology in the CMD of Galactic open clusters of different ages. Induced overshooting and semiconvection during the central He-burning phase are accounted for following Castellani et al. (1985).

Radiative opacities from the OPAL tables (Iglesias & Rogers 1996) for temperatures larger than 10^4 K, and from Alexander & Ferguson (1994) for lower temperatures, have been employed, supplemented by opacities for electron degenerate matter computed following Potekhin (1999). The relevant energy loss rate from plasma-neutrino processes comes from Haft, Raffelt & Weiss (1994), whereas for all other processes the reader is referred to Cassisi & Salaris (1997); the nuclear reaction rates are from the NACRE data base (Angulo et al. 1999), with the exception of the $^{12}\mathrm{C}(\alpha,\gamma)^{16}\mathrm{O}$ reaction, in which case the more accurate recent determination by Kunz et al. (2002) has been adopted. Electron screening is treated according to Graboske et al. (1973).

The accurate equation of state (EOS) by A. Irwin has been used. An exhaustive description of this EOS is in preparation (Irwin et al., in preparation) but a brief discussion of its main characteristics can be found in Cassisi et al. (2003). This EOS covers the full stellar structure for the whole evolutionary phase and mass range spanned by the model data base; in Pietrinferni et al. (2004) and Bahcall, Serenelli & Pinsonneault (2004) it is shown that this EOS and the latest version of the OPAL EOS (Rogers 2001) provide almost identical results in the case of the Sun. The accuracy and reliability of the present evolutionary scenario has been successfully tested in Cassisi et al. (2003), Riello et al. (2003) and Salaris et al. (2004) in the regime of GGCs, and by Pietrinferni et al. (2004) in the regime of field stars and open clusters. Cassisi et al. (2003) and Pietrinferni et al. (2004) have also compared our adopted set of theoretical isochrones with other existing isochrone data bases widely cited in the current literature. This comparison provides an estimate of the present uncertainties in stellar evolution models because of different choices for the stellar input physics (see also Chaboyer 1995). The main conclusions of this exercise are summarized below.

Isochrones for typical globular cluster ages (of the order of 10 Gyr) show a remarkable consistency for the prediction of the MS location and TO luminosity at a given initial chemical composition, whereas the RGB effective temperature and ZAHB brightness display values that differ by amounts of $\sim$100–200 K and $\sim$0.1 mag, respectively. Globular cluster ages estimated from the difference between TO and HB brightness would consequently be uncertain by $\sim$10 per cent (Chaboyer 1995 determined a similar uncertainty, of the order of 15 per cent).

Isochrones for ages lower than $\sim$4–5 Gyr show again consistent MS locations, but differing TO luminosities, effective temperatures and He-burning luminosities, due mainly to the uncertain treatment of the overshooting from the convective cores of the MS stars. These uncertainties cause variations in the estimated age of stellar

Table 2. Example of an isochrone available at http://www.te.astro.it/BASTI/index.php. Isochrone by Pietrinferni–Cassisi–Salaris–Castelli 2004 Standard Model. Scaled solar model and transformations for ACS. $Np = 2000$, [M/H] $= -0.659$, $Z = 0.0040$, $Y = 0.251$, t(Gyr) $= 11.0000$

$(M/M_\odot)_{in}$	$(M/M_\odot)$	$\log L/L_\odot$	$\log T_{eff}$	M_{F435W}	M_{F475W}	M_{F555W}	M_{F606W}	M_{F625W}	M_{F775W}	M_{F814W}
.5000000000	.4999030025	−1.20676	3.62790	9.540	9.063	8.418	8.024	7.693	7.069	6.982
.5011654487	.5011233468	−1.20259	3.62829	9.525	9.048	8.405	8.012	7.681	7.059	6.972
.5023308974	.5023308974	−1.19841	3.62868	9.510	9.034	8.392	8.000	7.670	7.049	6.962
...	...	...	...	...	...	...	...	...	...	...
.9066248329	.6047402926	2.89310	3.60793	−0.175	−0.871	−1.635	−2.045	−2.382	−3.053	−3.153
.9066266265	.6037663031	2.92275	3.60503	−0.190	−0.899	−1.675	−2.093	−2.435	−3.116	−3.218
.9066284200	.6026715201	2.95336	3.60202	−0.204	−0.926	−1.715	−2.143	−2.490	−3.181	−3.285

populations within this age range, of at most ∼30 per cent. Also, in this age range, the effective temperatures of red giants show a spread of ∼100–200 K.

3.2 Transformation to the observational plane

Here we describe the procedure we have followed to transform our models into the ACS Vega-mag system defined in Section 2.

We computed ACS colour indices by using the homogeneous set of ODFNEW model atmospheres and synthetic fluxes[7] (Castelli & Kurucz 2003) computed with the Kurucz ATLAS9 code. We generated grids of indices for the following values of [Fe/H]: 0.5, 0.2, 0.0, −0.5, −1.0, −1.5, −2.0 and −2.5.

In each grid point, T_{eff} ranges from 3500 to 50 000 K, $\log g$ from 0.0 to 5.0, and the microturbulent velocity is $\xi = 2.0\,km\,s^{-1}$. We tabulated for each T_{eff} and $\log g$ grid point the BC_V bolometric correction, the V magnitude and the colour indices $V–m_{F435W}$, $V–m_{F475W}$, $V–m_{F555W}$, $V–m_{F606W}$, $V–m_{F625W}$, $V–m_{F775W}$ and $V–m_{F814W}$. The ACS magnitudes were computed by using the WFC/ACS transmission curves described in Section 2.1, while we adopted the V passband from Bessell (1990).

We adopted $V = 0.03$ for Vega and set all colour indices $(V–m^{ACS}_{filter})$ to zero, so that the Vega ACS magnitudes would be equal to 0.00 in all passbands. The Vega model and flux are the ATLAS9 model and the ATLAS9 flux from Castelli & Kurucz (1994) with parameters $T_{eff} = 9550$ K, $\log g = 3.95$, [M/H] $= -0.5$, $\xi = 2$ km s^{-1}. Note that this model has been built specifically to reproduce the observations of the spectrum used in Section 2.2. The absolute zero-point for the V magnitude was fixed by adding the constant −21.10 mag to the computed V for Vega (Bessell, Castelli & Plez 1998).

In Table 2 we show an example of the theoretical isochrones transformed into the ACS Vega-mag photometric system. The header of the isochrone table provides information about the number of lines in the file (N_P), the total metallicity [M/H], the abundance by mass of metals (Z) and helium (Y), and the corresponding age in billions of years, t(Gyr). The content of the columns in the following lines is as follows (from left to right): column 1, the initial mass of each star; column 2, the current mass at the specified age (computed accounting for mass loss; see previous section); column 3, the logarithm of the surface luminosity in solar units; column 4, the logarithm of the effective temperature; column 5, the ACS M_{F435W} magnitude; column 6, the ACS M_{F475W} magnitude; column 7, the ACS M_{F555W} magnitude; column 8, the ACS M_{F606W} magnitude; column 9, the ACS M_{F625W} magnitude; column 10, the ACS M_{F775W} magnitude; column 11, the ACS M_{F814W} magnitude.

[7] Available at http://wwwuser.oat.ts.astro.it/castelli/grids.html.

The entire set of transformed isochrones, as well as the ZAHB and post-ZAHB evolutionary tracks, can be retrieved from http://www.te.astro.it/BASTI/index.php.

3.3 Reddening in the WFC/ACS Vega-mag system

Following the recipe and the motivations given by Holtzman et al. (1995), we also computed the interstellar absorption in the WFC/ACS bands as a function of $E(B–V)$. By using the extinction curve from table 1 in Mathis (1990) for $R_V = 3.1$ we computed, for different values of $E(B–V)$, the interstellar reddening A_λ at the wavelengths of the ATLAS9 flux, the corresponding reddened fluxes and the reddened WFC/ACS magnitudes. The A_{filter} extinctions in the WFC/ACS filters were obtained as differences between the reddened and unreddened m_{filter} magnitudes.

Tables 3 and 4 give the values of the A_{filter} for a cool star and a hot star, respectively. We give these values for the main filters: F435W, F475W, F555W, F606W, F625W, F775W and F814W. We note how these values are very close to those tabulated by Holtzman et al. (1995) for WFPC2's similar filters.

4 ACS VEGA-MAG SYSTEM ZERO-POINTS

Table 5 lists the zero-points for the ACS Vega-mag system in other useful passbands; the zero-points for all the other filters can be easily obtained following the recipes outlined above.

We note that this calibration is linked to the chosen spectrum of Vega. These zero-points are probably accurate to two to three hundredths of a magnitude, and can (and hopefully will soon) be updated, once more accurate data on the ACS performance are available.

The main sources of systematic error in the calibration of the observations are: residuals in correction for CTE, flat-fielding, aperture corrections, charge diffusion and the encircled energy, which seems to depend on stellar colour (Sirianni, private communication). Still, the lack of any other official and complete photometric calibration of the ACS, useful for the comparison with stellar models, has led us to calculate and publish this calibration.

In summary, photometric observations can be transformed into the ACS/WFC Vega-mag system defined in this paper by applying the following relation:

$$m_{filter} \equiv -2.5\,\log_{10}\,\frac{I_{e^-}}{exptime} + Zp^{filter} + \\ -\Delta m^{filter}_{PSF-AP(r)} - \Delta m^{filter}_{AP(r)-AP(\infty)}. \quad (1)$$

Here, r can assume the values: ∞, 0.5 arcsec or 0.3 arcsec. Note that the last two positive quantities in equation (1) are subtracted.

Table 3. Extinctions (in mag) in different ACS filters as a function of the colour excess $E(B–V)$ of a cool star. $T_{\rm eff} = 4000$ K, log $g = 4.50$, [M] $= 0.00$, $v_{\rm turb} = 2.00$, $l/H = 1.25$

$E(B–V)$	$A_{\rm F435W}$	$A_{\rm F475W}$	$A_{\rm F555W}$	$A_{\rm F606W}$	$A_{\rm F625W}$	$A_{\rm F775W}$	$A_{\rm F814W}$
0.00	0.000	0.000	0.000	0.000	0.000	0.000	0.000
0.05	0.202	0.182	0.158	0.140	0.132	0.099	0.092
0.10	0.404	0.365	0.316	0.279	0.263	0.198	0.184
0.15	0.606	0.546	0.474	0.419	0.394	0.297	0.276
0.20	0.808	0.728	0.632	0.558	0.526	0.396	0.367
0.25	1.010	0.909	0.790	0.696	0.657	0.495	0.459
0.30	1.212	1.090	0.947	0.834	0.788	0.594	0.550
0.35	1.413	1.271	1.104	0.972	0.919	0.692	0.641
0.40	1.614	1.451	1.262	1.110	1.050	0.791	0.732
0.45	1.815	1.631	1.419	1.248	1.180	0.890	0.823
0.50	2.017	1.811	1.575	1.385	1.311	0.988	0.913
0.55	2.217	1.990	1.732	1.522	1.442	1.086	1.004
0.60	2.418	2.169	1.889	1.658	1.572	1.185	1.094
0.65	2.619	2.348	2.045	1.794	1.702	1.283	1.184
0.70	2.819	2.527	2.201	1.930	1.833	1.381	1.274
0.75	3.020	2.705	2.357	2.066	1.963	1.479	1.364
0.80	3.220	2.883	2.513	2.202	2.093	1.577	1.454
1.00	4.020	3.592	3.136	2.741	2.612	1.968	1.811
1.25	5.016	4.472	3.911	3.409	3.260	2.454	2.254
1.50	6.010	5.347	4.682	4.072	3.905	2.939	2.693
1.75	7.001	6.215	5.450	4.730	4.547	3.422	3.128
2.00	7.990	7.077	6.216	5.382	5.188	3.902	3.559
2.25	8.975	7.935	6.978	6.031	5.827	4.381	3.987
2.50	9.959	8.788	7.737	6.675	6.463	4.858	4.411
2.75	10.940	9.636	8.494	7.315	7.098	5.333	4.832
3.00	11.919	10.480	9.249	7.951	7.731	5.806	5.250
3.25	12.896	11.320	10.001	8.585	8.362	6.277	5.664
3.50	13.871	12.157	10.751	9.215	8.991	6.747	6.075
3.75	14.844	12.991	11.499	9.843	9.619	7.215	6.483
4.00	15.815	13.822	12.244	10.468	10.245	7.681	6.888
4.25	16.785	14.650	12.988	11.091	10.870	8.145	7.291
4.50	17.753	15.476	13.730	11.711	11.493	8.608	7.690
4.75	18.719	16.299	14.470	12.329	12.115	9.070	8.088
5.00	19.684	17.120	15.209	12.946	12.735	9.530	8.483

Models can be transformed into the observational plane of the same system by applying

$$M_{\rm filter} = -2.5 \log_{10} \frac{I({\rm filter})}{I^0({\rm filter})}. \quad (2)$$

Here, the meanings of I(filter) and I^0(filter) are clear from the discussions in previous sections. In Section 5.2 we give a practical example of how to calibrate the observations.

Our zero-points agree well with those presented in the recent Instrument Science Report by De Marchi et al. (2004).[8] The only differences are a result of a different choice of spectrum of Vega (Sirianni, private communication). Nevertheless, for broad filters the zero-points agree within ∼0.005 mag.

5 COMPARISON OF MODELS WITH OBSERVATIONS

5.1 Observations and data reduction

In order to give a practical example of our procedures and to provide a useful test for our models, we used archival WFC observations of five GGCs (GO-9453; PI, Brown), which span a wide range in metallicity ($-2.2 <$ [Fe/H] < -0.04). The data are summarized in Table 6. They consist of one short, one intermediate and one (relatively) long exposure, in both F606W and F814W filters, for each cluster.

We carried out the photometry with algorithms based on the effective PSF (ePSF) fitting procedure described by Anderson & King (2000). We obtained the ePSF from a set of images from a different project using the same filters, because the dithering of GO-9453 images was unsuitable to constrain the ePSF shape (Anderson & King 2000).

The resampling present in the DRZ images provided by STScI does not allow the use of the ePSF method, limiting the precision of the output photometry. We therefore performed our fitting photometry using FLT images. These images, affected by geometrical distortion, have been flat-fielded to preserve surface brightness, but not flux. Therefore, we must multiply each pixel by its projected area to obtain a proper flux for each star.

We find slight differences of flux-scaling between our corrected FLT images and the corresponding DRZ images (of the order of 1 per cent or so). Because it is the DRZ images that have been carefully calibrated via the STScI pipeline, we should convert any photometry measured on FLT images into the corresponding infinite-aperture fluxes in the DRZ images. The photometry has been calibrated as described in the previous sections.

[8] See http://www.stsci.edu/hst/acs/documents/isrs/isr0408.pdf.

Table 4. As in Table 3, but for a hot star. $T_{\rm eff} = 40\,000$ K, log $g = 4.50$, [M] $= 0.00$, $v_{\rm turb} = 2.00$, $l/H = 1.25$

$E(B–V)$	$A_{\rm F435W}$	$A_{\rm F475W}$	$A_{\rm F555W}$	$A_{\rm F606W}$	$A_{\rm F625W}$	$A_{\rm F775W}$	$A_{\rm F814W}$
0.00	0.000	0.000	0.000	0.000	0.000	0.000	0.000
0.05	0.212	0.194	0.165	0.153	0.135	0.102	0.096
0.10	0.423	0.387	0.329	0.305	0.269	0.203	0.192
0.15	0.635	0.580	0.493	0.456	0.403	0.304	0.288
0.20	0.846	0.773	0.657	0.608	0.538	0.406	0.383
0.25	1.057	0.965	0.821	0.759	0.672	0.507	0.479
0.30	1.267	1.157	0.985	0.909	0.806	0.608	0.574
0.35	1.478	1.348	1.148	1.059	0.940	0.709	0.669
0.40	1.688	1.539	1.311	1.209	1.073	0.810	0.764
0.45	1.898	1.730	1.474	1.358	1.207	0.911	0.859
0.50	2.108	1.921	1.637	1.507	1.341	1.012	0.953
0.55	2.318	2.111	1.800	1.656	1.474	1.112	1.048
0.60	2.527	2.300	1.963	1.804	1.608	1.213	1.142
0.65	2.737	2.490	2.125	1.951	1.741	1.313	1.237
0.70	2.946	2.678	2.288	2.099	1.874	1.414	1.331
0.75	3.155	2.867	2.450	2.246	2.007	1.514	1.424
0.80	3.364	3.055	2.612	2.392	2.140	1.615	1.518
1.00	4.196	3.804	3.258	2.975	2.671	2.015	1.891
1.25	5.233	4.732	4.062	3.694	3.333	2.513	2.354
1.50	6.265	5.651	4.862	4.405	3.992	3.009	2.813
1.75	7.292	6.562	5.658	5.107	4.648	3.503	3.268
2.00	8.315	7.465	6.450	5.800	5.302	3.995	3.719
2.25	9.333	8.360	7.239	6.486	5.954	4.485	4.166
2.50	10.347	9.247	8.023	7.165	6.603	4.972	4.609
2.75	11.357	10.128	8.804	7.837	7.250	5.458	5.048
3.00	12.362	11.003	9.581	8.503	7.895	5.942	5.483
3.25	13.364	11.872	10.355	9.163	8.538	6.423	5.915
3.50	14.362	12.735	11.126	9.818	9.178	6.902	6.343
3.75	15.357	13.594	11.894	10.468	9.817	7.380	6.767
4.00	16.348	14.447	12.658	11.114	10.453	7.856	7.187
4.25	17.336	15.297	13.420	11.755	11.088	8.329	7.604
4.50	18.321	16.142	14.179	12.393	11.721	8.801	8.018
4.75	19.303	16.985	14.935	13.028	12.352	9.271	8.429
5.00	20.283	17.823	15.689	13.659	12.981	9.740	8.837

Table 5. Natural ACS-Vega system zero-points ($Zp^{\rm filter}$), and fluxes I^0(filter) (in 10^{-6} erg s^{-1} cm^{-2}).

Filter	$Zp^{\rm filter}$	I^0(filter)
F435W	25.785	2.0994
F475W	26.168	2.7611
F502N	22.338	0.075320
F550M	24.861	0.69396
F555W	25.718	1.6028
F606W	26.391	2.7591
F625W	25.722	1.3687
F658N	22.381	0.059770
F660N	21.342	0.022895
F775W	25.254	0.72740
F814W	25.492	0.87198

5.2 An example: calibration of the 47 Tuc photometry

For the GO-9453 47 Tuc data, the zero-point of the long exposures has been used to calibrate the intermediate and short exposures in both F606W (for which the exposure time is 70 s) and F814W filters (for which the exposure time is 72 s; see Table 3). We determined the zero-point difference between our PSF-fitting photometry and aperture photometry with a 0.5-arcsec aperture for each filter. The differences are $\Delta m^{\rm F606W}_{\rm PSF-AP(0.5\,arcsec)} = +\,0.15$ ($\pm$0.015) and $\Delta m^{\rm F814W}_{\rm PSF-AP(0.5\,arcsec)} = +\,0.25$($\pm$0.015). To these we need to add the aperture corrections. According to Table 1, $\Delta m^{\rm F606W}_{\rm AP(0.5\,arcsec)-AP(\infty)} = \Delta m^{\rm F814W}_{\rm AP(0.5\,arcsec)-AP(\infty)} = +\,0.079$ (equal for the two filters, at this aperture). In summary, from equation (1)

$$m_{\rm F606W} \equiv -2.5\log_{10}\,\frac{I_{\rm e^-}}{70} + 26.391 - 0.15 - 0.079$$

$$m_{\rm F814W} \equiv -2.5\log_{10}\,\frac{I_{\rm e^-}}{72} + 25.492 - 0.25 - 0.079.$$

[Note the following: (i) $-2.5\,\log_{10}\,I^-_{\rm e}$ is simply the instrumental magnitude (some codes, such as DAOPHOT, add a constant value of 25 to the instrumental magnitude to avoid negative numbers); (ii) the adopted normalization of the fitting magnitude is taken into account by the aperture correction $\Delta m_{{\rm PSF-AP}(r)}$; (iii) the sign of the last two quantities in each equation is negative.]

Table 6. Data set of the observed clusters.

Cluster	F606W data	F814W data
NGC 6528	4s, 50s, 450s	1s, 20s, 350s
NGC 5927	2s, 30s, 500s	0.7s, 15s, 340s
NGC 104	0.5s, 6s, 70s	0.5s, 5.5s, 72s
NGC 6752	0.5s, 4s, 40s	0.5s, 4s, 45s
NGC 6341	0.5s, 5s, 90s	0.5s, 6s, 100s

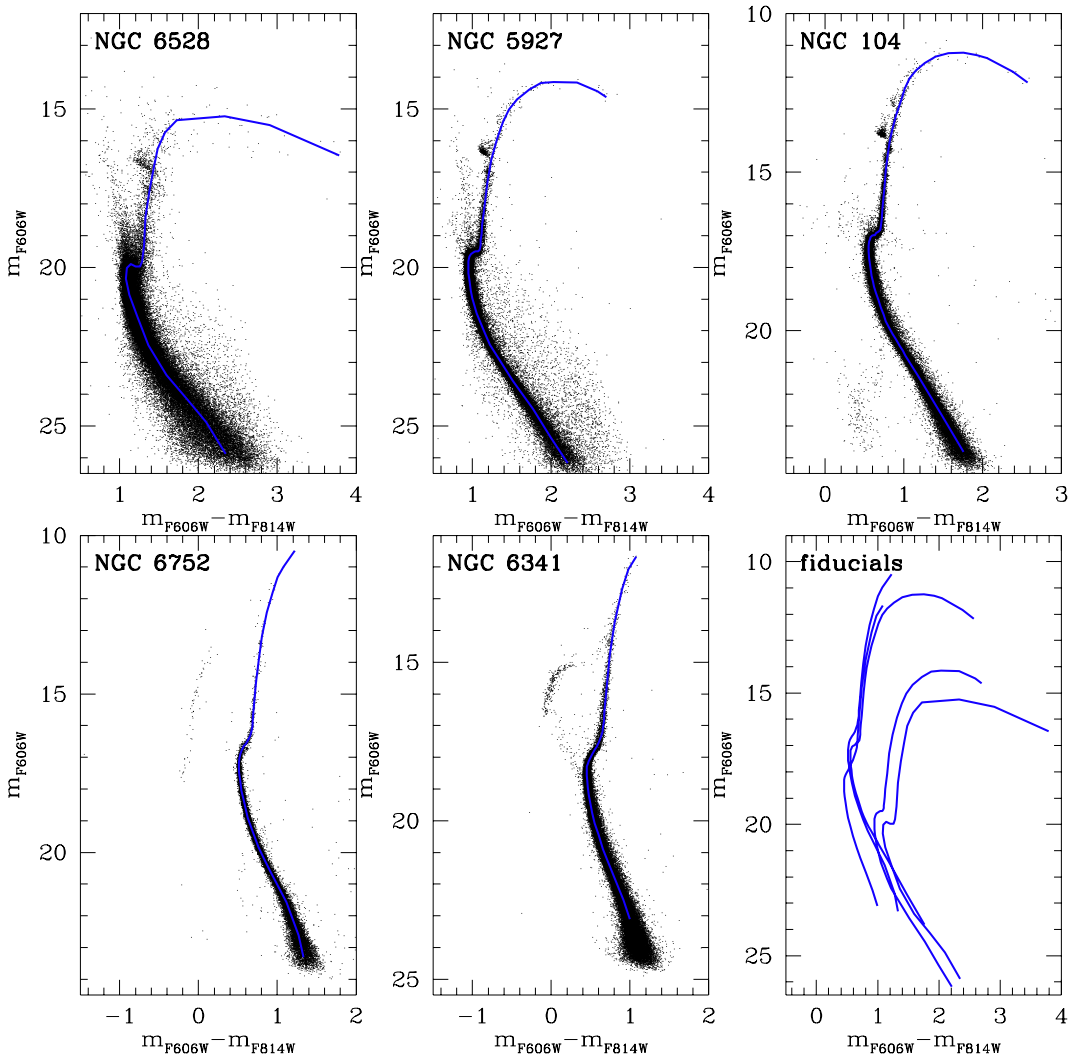

Figure 2. Observed CMDs for the five clusters discussed in the text and summarized in Table 6. The fiducials are overplotted on to each CMD, and shown together in the bottom-right panel for comparison.

The calibrated CMDs are presented in Fig. 2. Superposed on the observed CMD are the fiducial lines of the MS, Sub-giant branch (SGB) and RGB. The fiducial points which define them have been determined by eye and are given in Table 7. Note that, because of the differential reddening in the field, the fiducial lines in the cases of NGC 6528 and 5927 are poorly defined.

These fiducial points can be used as a reference to compare against those measured for other globular clusters or galaxies whose stars are resolved (Brown et al. 2003).

5.3 Comparison with the models

In this section we compare the theoretical models transformed to the ACS Vega-mag system with observed CMDs.

Fig. 3 displays our adopted α-enhanced isochrones and ZAHBs compared with the observed CMDs of the GGCs 47 Tuc (NGC 104), NGC 6752 and M92 (NGC 6341). These clusters span a wide metallicity range ($-2.2 < [Fe/H] < -0.6$). We selected these clusters for the comparison because of their very low extinction and lack of differential reddening.

In the following discussion, in order to make the comparison with the values in the literature more straightforward, we give the reddening $E(B–V)$ and the apparent distance modulus in the V band (y_V). The $E(B–V)$ comes from $E(m_{F606W} - m_{F814W}) = A_{F606W} - A_{F814W}$ as adopted in the best fit by interpolation of the values in Table 3. The y_V comes from the best-fitting distance modulus in the F606W band (y_{F606W}): $y_V = y_{F606W} - A_{F606W} + A_V$, where $A_V = 3.1\ E(B–V)$.

In the case of 47 Tuc we used α-enhanced ($\langle[\alpha/Fe]\rangle = 0.4$) isochrones with $[Fe/H] = -0.66$ ($Z = 0.008$), a value in very good agreement with spectroscopic measurements (see, for example, Percival et al. 2002; Gratton et al. 2003); the best match is obtained for an apparent distance modulus $y_V = 13.45$, an age of 10 Gyr, and a reddening $E(B–V) = 0.04$ (the 8- and 13-Gyr isochrones are also shown). These values of distance modulus and reddening are consistent with empirical determinations by Percival et al. (2002) and Gratton et al. (2003).

The quality of the fit is satisfactory along most of the isochrone, worsening at the redder end of both the RGB and MS. The deviation of the lower part of the sequence from the models for intermediate-metallicity clusters is well known (see Bedin et al. 2001).

For NGC 6752 we have employed our isochrones with $[Fe/H] = -1.26$ ($Z = 0.002$), a value close to the estimate by Rutledge, Hesser & Stetson (1997) with their calibration of the Ca II triplet

Table 7. Fiducial points in the plane: $(m_{\rm F606W} - m_{\rm F814W})$, $m_{\rm F606W}$.

Colour	Mag	Colour	Mag
NGC 6528		1.75	11.23
		1.56	11.25
3.79	16.46	1.40	11.36
2.91	15.52	1.27	11.55
2.33	15.24	1.16	11.78
1.72	15.36	1.07	12.03
1.57	15.75	1.01	12.35
1.48	16.26	0.94	12.84
1.43	16.85	0.88	13.32
1.38	17.59	0.83	13.83
1.33	18.41	0.80	14.26
1.31	19.33	0.76	14.90
1.28	19.82	0.74	15.55
1.26	19.97	0.73	15.98
1.20	19.97	0.71	16.37
1.14	19.89	0.71	16.58
1.09	20.02	0.70	16.74
1.08	20.35	0.69	16.81
1.12	20.86	0.67	16.90
1.23	21.58	0.65	16.95
1.36	22.45	0.62	16.99
1.60	23.40	0.59	17.06
1.85	24.14	0.57	17.16
2.10	24.88	0.56	17.30
2.35	25.88	0.56	17.52
NGC 5927		0.56	17.76
2.70	14.63	0.57	18.01
2.59	14.45	0.59	18.33
2.33	14.17	0.62	18.67
2.03	14.15	0.67	19.07
1.87	14.18	0.73	19.50
1.72	14.38	0.82	19.96
1.57	14.69	1.02	20.77
1.46	15.02	1.18	21.45
1.39	15.40	1.47	22.65
1.31	15.93	1.76	23.82
1.24	16.59	NGC 6752	
1.18	17.18	1.22	10.48
1.15	17.84	1.08	10.99
1.12	18.53	1.00	11.32
1.12	18.94	0.94	11.80
1.11	19.21	0.87	12.42
1.10	19.32	0.81	13.19
1.08	19.44	0.77	13.88
1.04	19.49	0.73	14.60
1.01	19.52	0.71	15.10
0.97	19.64	0.69	15.60
0.95	19.75	0.68	15.91
0.95	20.00	0.66	16.15
0.95	20.33	0.65	16.35
0.98	20.66	0.64	16.44
1.01	21.09	0.61	16.51
1.08	21.63	0.58	16.66
1.23	22.44	0.55	16.78
1.51	23.58	0.53	16.87
1.77	24.47	0.52	17.02
1.99	25.36	0.51	17.16
2.21	26.18	0.51	17.33
NGC 104		0.52	17.61
2.57	12.17	0.53	17.83
2.38	11.83	0.56	18.26
2.05	11.39	0.60	18.67
1.92	11.30	0.66	19.17
0.78	19.93	0.55	17.76
0.93	20.63	0.52	17.91
1.12	21.56	0.49	18.03
1.27	22.61	0.48	18.12
1.33	23.31	0.46	18.21
NGC 6341		0.45	18.30
1.08	11.67	0.45	18.42
0.98	12.06	0.45	18.58
0.90	12.70	0.45	18.74
0.80	13.73	0.46	18.93
0.74	14.77	0.48	19.18
0.72	15.41	0.49	19.43
0.69	16.06	0.52	19.75
0.68	16.54	0.55	20.08
0.67	16.86	0.60	20.44
0.66	17.07	0.66	20.90
0.65	17.22	0.72	21.29
0.63	17.34	0.81	21.85
0.60	17.55	0.92	22.51
0.57	17.68	1.00	23.11

index on the GGC Carretta & Gratton (1997) metallicity scale. We obtain a best match with $y_V = 13.25$, an age of 12 Gyr and $E(B–V) = 0.04$ (the 10- and 14-Gyr isochrones are also shown).

Again, the reddening agrees with independent empirical estimates (e.g. Gratton et al. 2003), whereas the distance is slightly longer than the MS-fitting estimates (Carretta et al. 2000; Gratton et al. 2003). These empirical estimates employ a metallicity ∼0.2 dex lower than our adopted value; it is interesting to note, judging from the numerical experiment performed by Carretta et al. (2000, see their fig. 5), that their empirical MS-fitting distance would come into agreement with our value if our assumed metallicity is used in their MS-fitting technique.

Had we used our isochrones for $[{\rm Fe/H}] = -1.57 (Z = 0.001)$ and a value close to the metallicity estimate by Rutledge et al. (1997), obtained by calibrating the calcium index on the Zinn & West (1984) metallicity scale, the quality of the fit to the RGB location would be worse (isochrone too blue), the age older by ∼1 Gyr, $E(B–V) \sim 0.02$ mag higher and $y_V \sim 0.07$ mag larger.

The comparison with the M92 (NGC 6341) CMD has been performed using isochrones with $[{\rm Fe/H}] \approx -2.1 (Z = 0.0003)$, a value in fair agreement with the estimate by Carretta & Gratton (1997) ($[{\rm Fe/H}] = -2.16$). The best agreement is achieved for an age of 12 Gyr, $E(B–V) = 0.04$ and $y_V = 14.85$ (the 10- and 14-Gyr isochrones are also shown).

6 SUMMARY

In this paper we have proposed a simple zero-point photometric calibration of the ACS/WFC data, based on a model spectrum of Vega and the most up-to-date in-flight transmission curves of the ACS camera. We have named this new in-flight system the WFC/ACS Vega-mag photometric system. The proposed calibration is accurate at the level of a few hundredths of a magnitude. We give the basic recipes to calibrate both the observed data and the models, and we present a set of models by Pietrinferni et al. (2004) already transformed into the new ACS Vega-mag system.

Because the primary purpose of this investigation is to make available to the public a complete set of stellar models and isochrones

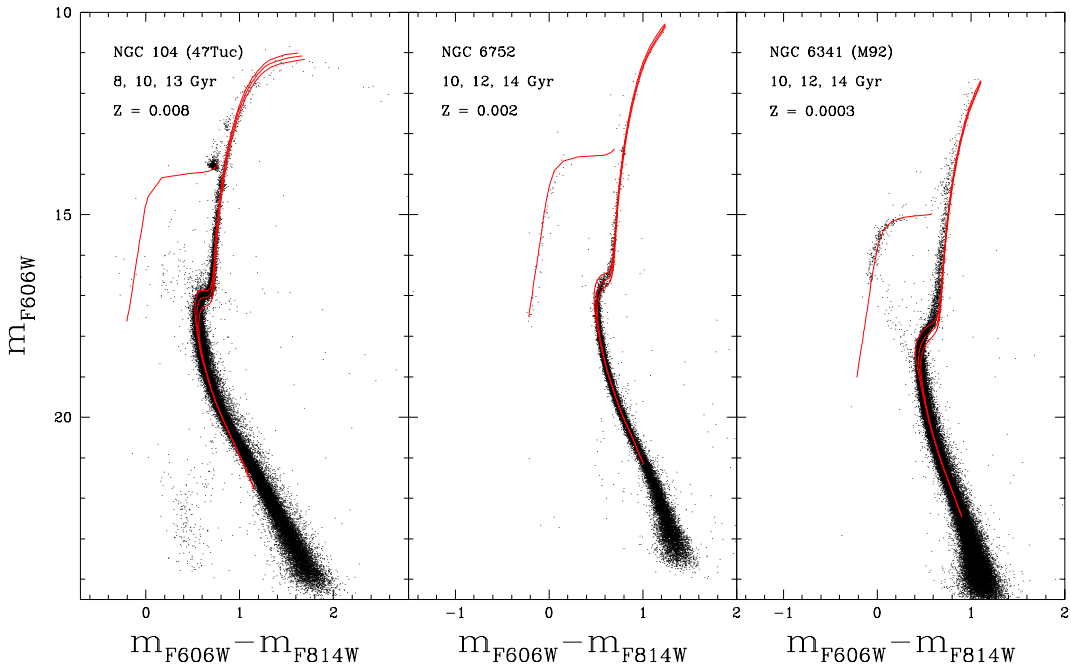

Figure 3. Comparison of three GGCs CMDs (M92, NGC 6752 and 47 Tuc) with the corresponding isochrones (see text for details).

transformed to the ACS Vega-mag system, we have developed the following website where all models and isochrones can be retrieved: http://www.te.astro.it/BASTI/index.php.

We show CMDs for five GGCs, spanning a metallicity range $-2.2 < [Fe/H] < -0.04$; these CMDs have been obtained from ACS observations, calibrated to the ACS Vega-mag system, and used to test our models. We also give the fiducial points representing their RGB, SGB and MS from the RGB tip to several magnitudes below the TO. These CMDs and fiducial points will be useful for the study of the old stellar populations in other stellar systems (Brown et al. 2003).

ACKNOWLEDGMENTS

This work is based on observations with the NASA/ESA *HST*, obtained at the Space Telescope Science Institute, which is operated by the Association of Universities for Research in Astronomy (AURA), Inc., under NASA contract NAS 5-26555. We are very grateful to Marco Sirianni for providing us with the ACS/WFC transmission curves, and also for discussions. We thank the anonymous referee for useful suggestions, James Manners for a careful reading of the manuscript, and Phil James for polishing it. This work has been partially supported by the Agenzia Spaziale Italiana and by the Ministero dell'Istruzione, Università e Ricerca under the programme PRIN2003.

REFERENCES

Alexander D. R., Ferguson J. W., 1994, ApJ, 437, 879
Anderson J., King I. R., 2000, PASP, 112, 1360
Angulo C. et al. (NACRE Collaboration), 1999, Nucl. Phys. A, 656, 3
Bahcall J. N., Serenelli A. M., Pinsonneault M., 2004, ApJ, 614, 464
Bedin L. R., Anderson J., King I. R., Piotto G., 2001 ApJ, 560, L75
Bessell M. S., 1990, PASP, 102, 1181
Bessell M. S., Castelli F., Plez B., 1998, A&A, 333, 231
Böhm-Vitense E., 1958, Z. Astrophys., 46, 108
Brown T., Ferguson H. C., Smith E., Kimble R. A., Sweigart A. V., Renzini A., Rich R. M., VandenBerg D. A., 2003, ApJ, 592, L17
Carretta E., Gratton R. G., 1997, A&AS, 121, 95
Carretta E., Gratton R. G., Clementini G., Fusi Pecci F., 2000, ApJ, 533, 215
Cassisi S., Salaris M., 1997, MNRAS, 285, 593
Cassisi S., Salaris M., Irwin A. W., 2003, ApJ, 588, 862
Castellani V., Chieffi A., Pulone L., Tornambé A., 1985, ApJ, 296, 204
Castelli F., Kurucz R. L., 1994, A&A, 281, 817
Castelli F., Kurucz R. L., 2003, in Piskunov N., Weiss W. W., Gray D. F., eds, Proc. IAU Symp. 210, Modelling of Stellar Atmospheres, Poster A20 (astro-ph/0405087)
Chaboyer B., 1995, ApJ, 444, L9
Cox J. P., Giuli R. T., 1968, in Principles of Stellar Structure, Vol. II. Gordon & Breach, London
De Marchi G. et al., 2004, Instrument Science Report ACS 2004-08
Graboske H. C., Dewitt H. E., Grossman A. S., Cooper M. S., 1973, ApJ, 181, 457
Gratton R. G., Bragaglia A., Carretta E., Clementini G., Desidera S., Grundahl F., Lucatello S., 2003, A&A, 408, 529
Grevesse N., Noels A., 1993, in Prantzos N., Vangioni-Flam E., Cassé M., eds, Origin and Evolution of the Elements. Cambridge Univ. Press, Cambridge, p. 14
Haft M., Raffelt G., Weiss A., 1994, ApJ, 425, 222
Holtzman J. A., Burrows C. J., Casertano S., Hester J. J., Trauger J. T., Watson A. M., Worthey G., 1995, PASP, 107, 1065
Krishna-Swamy K. S., 1966, ApJ, 145, 174
Krist J., 2003, Instrument Science Report ACS 2003-06
Kunz R., Fey M., Jaeger M., Mayer A., Hammer J. W., Staudt G., Harissopulos S., Paradellis T., 2002, ApJ, 567, 643
Iglesias C. A., Rogers F. J., 1996, ApJ, 464, 943
Landolt A.U., 1992, AJ, 104, 340
Mathis J. S., 1990, ARA&A, 28, 37
Momany Y., Cassisi S., Piotto G., Bedin L. R., Ortolani S., Castelli F., Recio-Blanco A., 2003, A&A, 407, 303
Percival S. M., Salaris M., van Wyk F., Kilkenny D., 2002, ApJ, 573, 174
Pietrinferni A., Cassisi S., Salaris M., Castelli F., 2004, ApJ, 612, 168
Potekhin A. Y., 1999, A&A, 351, 787

Reimers D., 1975, Mem. Soc. R. Sci. Líege, 8, 369
Riello M. et al., 2003, A&A, 410, 553
Riess A., Mack J., 2004, Instrument Science Report ACS 2004-006
Rogers F. J., 2001, Contrib. Plasma. Phys., 41, 179
Rutledge G. A., Hesser J. E., Stetson P. B., 1997, PASP, 109, 907
Salaris M., Riello M., Cassisi S., Piotto G., 2004, A&A, 420, 911
Sirianni M., De Marchi G., Gilliland R., Bohlin R., Pavlovsky C., Mack J., 2002, in Arribas S., Koekemoer A., Whitmore B., eds, HST Calibration Workshop 2002. STScI, Baltimore, p. 13
Spergel D. N. et al., 2003, ApJS, 148, 175
Zinn R., West M. J., 1984, ApJS, 55, 45

This paper has been typeset from a TEX/LATEX file prepared by the author.